macromol

MDPI

Article

Co-Assembled Nanogels of Tannic Acid and Biocompatible Random Copolymers for Potential Ovalbumin Delivery

Antiopi Vardaxi [1,2] and Stergios Pispas [1,*]

[1] Theoretical and Physical Chemistry Institute, National Hellenic Research Foundation, 48 Vassileos Constantinou Avenue, 11635 Athens, Greece; avardaxi@eie.gr
[2] Department of Chemistry, National and Kapodistrian University of Athens (NKUA), 15784 Athens, Greece
* Correspondence: pispas@eie.gr; Tel.: +30-210-727-3824

Abstract

This study investigates the efficacy of co-assembled, physically cross-linked nanocarriers comprising tannic acid (TA) and a P(DMAEMA-co-OEGMA) random/statistical double-hydrophilic copolymer for ovalbumin (OVA) encapsulation. TA-based nanocarriers, prepared at varying TA molar ratios (10% *w*/*v* and 20% *w*/*v*), exhibited nanoaggregates of different sizes, as revealed by dynamic light scattering, with Nanocarrier 1 system showing populations of 11 and 109 nm, while Nanocarrier 2 formed a single population of 75 nm in size. Notably, both colloidal systems demonstrated stability under thermal treatment and resilience to changes in salt concentrations higher than 0.15 M, but disassembly phenomena in basic media. Utilizing these nanocarriers for OVA loading via electrostatic interactions revealed strong positive charges (~30 mV) for all protein-loaded nanocarrier cases. In particular, they demonstrated sizes within the desired range (R_h = 96–118 nm) and considerable stability over 20 days and in the presence of serum proteins. Overall, this study underscores the importance of physical cross-linking as a viable strategy for the formation of tunable nanometric hydrocolloids for effective protein encapsulation, with significant implications for drug delivery systems.

Keywords: tannic acid; ovalbumin; nanocarriers; biocompatible random copolymer; polymer hydrocolloids; physical cross-linking

1. Introduction

Protein and peptide drugs have been at the forefront of treatment for life-threatening diseases as a result of their enhanced selectivity and efficient pharmacological activity [1]. However, their physical instability and vulnerability to environmental conditions that could cause unfavorable denaturation and thus quick elimination from the bloodstream limit their therapeutic potential [2]. PEGylation is widely applied as a shielding process of proteins to prevent immunogenicity and breakdown [3]. The FDA has approved the clinical use of many PEGylated protein products [4]. Yet since functional groups of proteins (carboxyl, amine and thiol groups) are required for the PEG conjugation, this covalent interaction may cause steric interference, diminishing the overall protein molecule's bioactivity [5].

Scientists have developed case-by-case strategies to improve protein delivery. Delivery nanocarriers composed of organic or inorganic materials can be customized to ameliorate the pharmacokinetic and physicochemical profile of proteins and to efficiently release them to the target site without causing toxic effects [6]. Liposomes, for instance, enable the

Check for updates

Academic Editor: Ana María Díez-Pascual

Received: 22 December 2025
Revised: 13 January 2026
Accepted: 3 March 2026
Published: 10 March 2026

Copyright: © 2026 by the authors. Licensee MDPI, Basel, Switzerland. This article is an open access article distributed under the terms and conditions of the Creative Commons Attribution (CC BY) license.

physical encapsulation of hydrophobic/hydrophilic compounds [7], whereas polymeric nanocarriers can be used for polymer–protein bioconjugation, or protein encapsulation through physical embedding or chemical bonding [8]. Moreover, polyphenols are one of the most intriguing vectors that have recently attracted attention. Polyphenols are made up of hydrophilic and hydrophobic groups, and they can interact non-covalently to form complexes with proteins and DNA, among other biomacromolecules [9]. Their biological use is widespread since they are naturally biosynthesized and extracted from plants with sustainable and eco-friendly approaches [10]. Amphiphilic substances such as tannic acid (TA) are promising polyphenols that can encapsulate biomolecules through hydrogen bonding and hydrophobic interactions thanks to the presence of functional moieties (hydroxyl groups and aromatic rings). TA has low viscosity and enhanced solubility, and it can increase the solubilization of different hydrophobic substances such as curcumin, paclitaxel and amphotericin B [11]. Moreover, TA can readily bind to extracellular matrices (ECMs), including collagen and elastin, and create complexes with therapeutic proteins in aqueous solution, enabling their transport to ECMs in the heart [12]. On the other hand, TA lacks targeting abilities as it can indiscriminately interact with a wide range of biological constituents. This could restrict the use of protein/TA complexes for intravenous injection distribution to other target locations, like solid tumors. Therefore, even though TA possesses naturally desirable nanocarrier features, alternative approaches to modulate TA and biological component interactions are needed for any further use of this plant-based derivative for protein delivery purposes [9].

TA acts as a biopolymer cross-linker or as an additive to produce biomaterials such as hydrogels. The self-assembled non-covalently cross-linked networks arise from hydrogen bonding and acid–base interactions [10]. In this regard, chitosan has been widely studied since its amine groups can non-covalently interact with the hydroxyl moieties of TA. At the macroscale, the chitosan–tannic acid physical cross-linking can produce hydrogels and films with different adhesion and swelling behaviors, whilst at the nanoscale it can determine the loading and release ratio of a therapeutic substance [13,14].

To the best of our knowledge, while many natural polysaccharides and other biopolymers have been extensively studied as TA-interacting counterparts, there are only a few reports of synthetic biocompatible copolymer utilization in such systems. In this regard, synthetic copolymers enable precise control over molecular-weight distribution and polymer composition, charge density, hydrophilic–hydrophobic balance, and responsiveness to external stimuli, which are important parameters in protein/drug delivery system design. Poly(2-(dimethylamino)ethyl methacrylate) (PDMAEMA) is a weak polyelectrolyte that exhibits pH- and temperature-responsive behavior and is capable of forming electrostatic and hydrogen bonding interactions with polyphenols such as TA [15,16]. Oligo(ethylene glycol) methacrylate (OEGMA) oligomer, as an alternative to PEG, enhances the hydrophilicity, steric stabilization and colloidal stability, offering shielding properties to the nanocarriers that are used [5]. The combination of these two monomeric units into a random/statistical copolymer, therefore, provides a versatile platform for exploring non-covalently cross-linked TA-based nanocarriers with tunable physicochemical characteristics.

This study aims to produce TA-based nanocarriers for protein delivery by leveraging the non-covalent interaction between the biocompatible P(DMAEMA-co-OEGMA) random/statistical copolymer and TA to ameliorate the colloidal stability of the system. The self-assembled non-covalent cross-linking led to the creation of nanoaggregates of different sizes, with stimuli responsiveness that depends on the biopolymer/cross-linker ratio. These nano-assemblies were further studied as candidates for ovalbumin (OVA) loading via electrostatic complexation and co-assembly. The complexation process was evaluated

from a physicochemical perspective using dynamic and electrophoretic light scattering techniques (DLS/ELS), as well as fluorescence, UV-Vis and ATR-FTIR spectroscopies.

2. Materials and Methods

2.1. Materials and Physically Cross-Linking

The linear double-hydrophilic random copolymer poly(2-(dimethylamino)ethyl methacrylate-co-(oligo ethylene glycol)methacrylate) (P(DMAEMA-co-OEGMA)) (M_w = 2.28 × 10^4 g/mol, M_w/M_n = 1.26, 76% wt. DMAEMA, 24% wt. OEGMA, (M_n of OEGMA monomer = 950 g/mol)), was synthesized using RAFT polymerization and described in detail in our previous publication [17]. Briefly, 4-Cyano-4-(dodecylsulfanylthiocarbonyl)pentanoic acid (CDP), as a chain transfer agent, and 2,2-Azobis (isobutyronitrile) (AIBN), as initiator, were utilized at a 10:1 ratio and mixed under magnetic stirring with purified DMAEMA and OEGMA monomers and 1,4 dioxane solvent (20% wt. monomer solution). All monomers, CDP, AIBN and solvents were purchased from Sigma-Aldrich (Darmstadt, Germany). The polymerization reaction was conducted at 70 °C for 24 h under nitrogen atmosphere. The final product was purified through dialysis against deionized H_2O and the pure copolymer was stored at 2–8 °C for further applications. The tannic acid (TA) was purchased from Sigma-Aldrich (Darmstadt, Germany). The polymer and tannic acid stock solutions, as well as the dilution of the final solutions, were prepared utilizing sterile water for injection obtained from DEMO S.A, Krioneri, Greece. For the preparation of TA-based nanocarriers, aliquots of tannic acid (0.1% *w*/*v*) were injected into the polymer solution (0.1% *w*/*v*) under rigorous magnetic stirring (900 rpm). The final aqueous solutions were diluted until V_{final} = 10 mL and left overnight to reach an equilibrium state. The tannic acid was added at 10% *w*/*v* and 20% *w*/*v* ratios and the Nanocarrier 1 and Nanocarrier 2 systems, respectively, were prepared. Three different preparations were performed and analyzed.

2.2. Physicochemical Characterization of TA-Based Nanocarriers

The physicochemical studies were conducted on stock solutions of concentrations ~1 × 10^{-4} g/mL. Using the dynamic light scattering technique (DLS), the scattered intensity and hydrodynamic radius changes were used to examine the nanocarriers' responsiveness to changes in solution pH, temperature, and salinity. For the pH-responsiveness studies, stock solutions at pH= 3, 7, and 10 were created for each nanogel solution by buffering an appropriate volume of HCl (0.01 M) and NaOH (0.01 M) solutions. The temperature-responsiveness was investigated by subjecting the neutral solutions of nanocarriers to a range of temperatures (from 25 to 55 °C with a 5 °C step). Moreover, the ionic strength studies were conducted through consecutive titration with a NaCl 1 M solution (salt concentration range achieved from 0.01 M to 0.5 M).

2.3. OVA Complexation with TA-Based Nanocarrier

The ovalbumin (OVA) (purchased from Serva, Heidelberg, Germany) solution (0.1% *w*/*v*) was injected into the nanogel solution at 10% wt. and 20% wt. mass relative to that of the nanocarriers. The mixtures were diluted with H_2O for injection to adjust the V_{final} = 10 mL and then remained for 20 min under gentle stirring. The formed complexes are presented with the names Nanocarrier 1-10, Nanocarrier 1-20, Nanocarrier 2-10 and Nanocarrier 2-20 for the complexes between Nanocarrier 1 and 2 with OVA at 10% wt. and 20% wt., respectively. The physicochemical behavior of the complexes was studied after the systems were left overnight to equilibrate.

2.4. Physicochemical Studies of Complexed Nanogels and FBS Interactions

The temperature responsiveness (temperature range: 25–55 °C with a 5 °C step) and ionic strength (titrations with NaCl 1 M at salt concentrations from 0.05 M to 0.5 M) of the complexed nanogels were evaluated utilizing the dynamic light scattering technique. Moreover, the FBS interactions with the complexed nanogels were examined. Briefly, the complexed nanogel solutions were added at a 1:1 ratio to FBS/PBS mixed solutions, which were prepared at 1:1 and 1:10 FBS/PBS ratios. The mixtures were measured through DLS after 1 h of interaction at t = 25 °C and T = 37 °C and compared with the particle size distributions of the FBS-filtered solution.

2.5. Characterization Techniques

2.5.1. Light Scattering Studies

An ALV/CGS-3 compact goniometer system (ALVGmbH, Langen, Germany) with a multi-τ digital correlator and a He-Ne laser light source (λ = 632.8 nm) was utilized for the dynamic light scattering studies. Hydrophilic 0.45 μm PVDF membrane filters were used to filter the solutions in order to eliminate any dust or large particles. Upon collecting the intensity autocorrelation functions (G(2)(t,q)) at a 90° angle, the CONTIN algorithm was applied to calculate the distribution of the typical decay time (τ). Using the Stokes–Einstein equation (Equation (1)) and the equation $\tau^{-1}(q) = Dq^2$, the distribution of the hydrodynamic radius f(R_h) was computed.

$$R_h = \frac{k_B T}{6\pi\eta D} \quad (1)$$

$$q = \frac{4\pi n_0}{\lambda} \sin\frac{\theta}{2} \quad (2)$$

where T is the absolute temperature, η is the solvent viscosity, n_0 is the solvent refractive index, and k_B is the Boltzmann constant. The average hydrodynamic radius of the species is determined by taking the maximum of the size distribution. The average scattered light intensity was simultaneously recorded, and served as a measure for the variation in the mass of the species in solution.

The ζ-potential measurements were carried out with a Zetasizer Nano ZS (Malvern Instruments, Worcestershire, UK) and they were computed using the Henry equation under the Smoluchowski approximation based on the electrophoretic mobility measurement. The results consist of averages from 50 scans conducted at a scattering angle of θ = 173°. To prevent multiple scattering effects, the DLS and ζ-potential were measured in diluted aqueous solutions (1:10 dilution ratio).

2.5.2. Fluorescence Spectroscopy

Measurements of fluorescence spectroscopy (Jobin Yvon Fluorolog-3 spectrofluorometer model GL3-21, Kyoto, Japan) utilizing the pyrene assay (excitation wavelength of 335 nm) were performed in order to assess the TA-based nanocarrier's internal micropolarity. The hydrophobic probe was added to the nanogel solutions (1 μL of 1 mM pyrene solution in acetone for 1 mL polymer solution) and allowed to equilibrate. Furthermore, the tryptophan residue excitation wavelength of 295 nm was used to assess the intrinsic fluorescence spectra of ovalbumin upon complexation with the nanogels.

2.5.3. UV-Vis Spectroscopy

Protein conformation was examined using UV–vis spectroscopy (Perkin Elmer Lambda 19 UV–Vis–NIR spectrometer, Waltham, MA, USA). The absorption fingerprint was analyzed between 200 and 800 nm to detect the distinctive absorption of the aromatic

amino acids tryptophan, tyrosine and phenylalanine (λ = 275–280 nm) and tannic acid (λ = 276 nm).

2.5.4. ATR-FTIR Spectroscopy

The secondary structure of the OVA protein in the complexed nanogels was confirmed using ATR-FTIR spectroscopy. FTIR spectra were acquired on a Bruker Optik Fourier transform instrument (Ettlingen, Germany) equipped with a press and an attenuated total reflectance diamond accessory, wherein many drops of the solution were deposited. The spectra of the aqueous solutions were recorded in the wavelength range of 550–4000 cm^{-1} at 2 resolution and 90 scans for each measurement while drying under nitrogen flow.

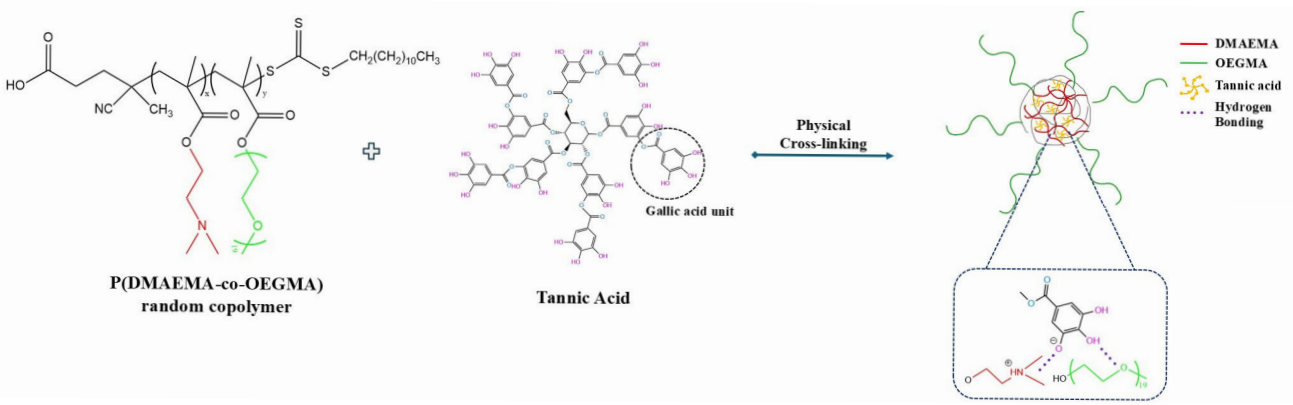
3. Results

3.1. Effect of the Non-Covalent Interaction on TA-Based Nanocarriers Physicochemical Characteristics

The simple synthetic route towards TA-based nanocarriers was facilitated by the self-assembly behavior of the double-hydrophilic random copolymer studies, which were presented in our previous publication [17]. The dual-responsive poly(2-(dimethylamino)ethyl methacrylate-co-(oligo ethylene glycol)methacrylate) (P(DMAEMA-co-OEGMA)) copolymer comprises DMAEMA and OEGMA segments. The dimethylamino groups (-$N(CH_3)_2$) can interact non-covalently with the phenolic acidic groups (-OH) of TA, forming amphiphilic cross-linked networks, while the non-ionic hydrophilic OEGMA segments provide shielding properties and colloidal stability [16,18]. Moreover, the aromatic rings located on galloyol phenols of TA can hydrophobically interact with the hydrophobic polymer backbones. Notably, several studies have effectively assessed the in vivo biocompatibility of random copolymers comprising either DMAEMA or OEGMA monomers, which can serve as biomolecule nanocarriers [19,20]. Chrysostomou et al. produced polyplexes of DMAEMA/OEGMA and QDMAEMA/OEGMA as non-viral gene delivery nanocarriers that displayed promising biocompatibility on breast cancer cell lines with high cell viability rates, including 4T1, MDA-MB-231, MCF-7, and T47D [21].

Based on the functional groups of P(DMAEMA-co-OEGMA) copolymer and the anchoring motif of TA, nanogel-like nanocarriers can be created through hydrogen bonding, acid–base interactions, and hydrophobic interactions between copolymer chains and TA. This intermolecular cross-linking can lead to the formation of a network structure, which may affect the physical properties of the collecting material, such as its swelling ratio and colloidal stability. These properties can be further tailored via TA addition at different ratios. For this reason, experiments on various TA–copolymer mixing ratios were carried out to assess the impact of TA concentration on the creation and stabilization of nanogels. In this study, homogeneous cloudy solutions of different turbidity were obtained after aliquots of 10% (*w*/*v*) and 20% (*w*/*v*) TA aqueous solutions were injected into the polymer aqueous solutions under vigorous stirring (900 rpm). Nanocarrier 1 refers to the mixture including 10% *w*/*v* TA, while Nanocarrier 2 refers to the one containing 20% *w*/*v* TA. Higher turbidity was detected in Nanocarrier 2 as a result of the augmented molar mass of the TA biopolymer cross-linker. Moreover, the turbidity was evidence of strong supramolecular bonding between the polymer aggregates and TA [22]. It should be noted that the TA contents of 10% and 20% *w*/*v* were selected based on preliminary screening studies, as these ratios provided stable and reproducible nanocarrier formation while avoiding the insufficient physical cross-linking at lower TA contents or aggregation with colloidal instability over time at higher TA concentrations. Nonetheless, lower-speed stirring trials revealed heterogeneous solutions comprising formulations that subsequently sedimented, thus confirming the effect of stirring on nanogel formation. These trials, which were carried out as part of the experimental design to assess the optimal compounding conditions, are

not included in the study that is being presented. The suggested interaction mechanism for the TA-based nanocarriers is depicted in Scheme 1.



Scheme 1. Schematic illustration of P(DMAEMA-co-OEGMA)/TA nanogel-like nanocarrier formation as a result of physical cross-linking between copolymer chains and TA molecules.

ATR-FTIR measurements were carried out to confirm the non-covalent cross-linking interactions between the biocompatible copolymer and TA (Figure 1). The broad vibration at 3070–2846 cm^{-1} is potentially attributed to hydrogen bonding between the phenolic hydroxyl groups of tannic acid and the tertiary amine groups of the DMAEMA segments and to possible electrostatic interactions between protonated DMAEMA and deprotonated TA. The remaining chemical groups in the fingerprint region are associated with the P(DMAEMA-co-OEGMA) copolymer. In particular, the strong vibration of a carbonyl moiety (C–O) is observed at 1728 cm^{-1}, whereas the stretching vibrations of a tertiary amine group (–$N(CH_3)_2$) are observed at 2821 and 2769 cm^{-1}. At 1459 cm^{-1}, the ether group (C-O-C) of the OEGMA segment is observed. The absence of new peaks or disappearance of characteristic ones confirms that nanocarrier formation proceeds via physical cross-linking rather than covalent bond formation.

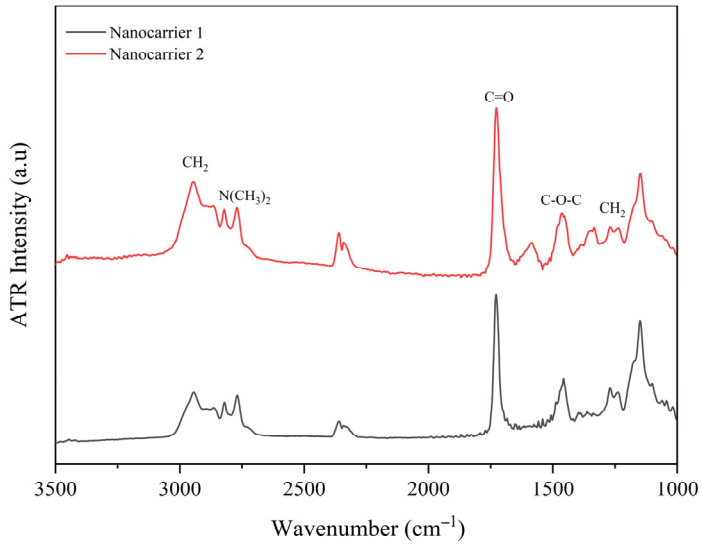


Figure 1. ATR-FTIR spectrum of Nanocarrier 1 and Nanocarrier 2 systems.

Our previous research on the self-assembly characteristics of P(DMAEMA-co-OEGMA) copolymers highlighted that temperature fluctuations, elevated salinity, and variations in pH of the surrounding environment can promote further aggregation and conformational state changes [17]. The homopolymer DMAEMA is a weak polyelectrolyte with pKa = 7.4

and LCST~50 °C (lower critical solution temperature point) constituted by a tertiary amine functional group, which is ionization-prone. The tertiary amino groups of the DMAEMA segments that either intermolecularly bond with the hydroxyl groups of TA or do not (i.e., remain as free dimethyl amino groups [15,17]) are responsible for the sensitivity of the TA-based nanocarriers to temperature and pH. Acknowledging that the polymers made of DMAEMA segments are expected to exhibit different self-assembly behavior in response to stimuli, light scattering techniques have been utilized to thoroughly investigate the nanocarriers produced by the non-covalent self-assembly of P(DMAEMA-co-OEGMA) copolymer and TA.

Dynamic light scattering (DLS) studies were carried out to provide insights into the particle size distributions and to assess the effects of different stimuli upon which conformational alterations occur (e.g., heating–cooling cycle). As depicted in Figure 2a, smaller particle sizes (R_h = 9 to 19 nm) in the case of Nanocarrier 1 were detected. Their absence at 45 °C and above, along with a significant increase in scattered intensity (I), suggested sudden changes related to structural changes in the co-assembled system and its conformation/aggregation in solution. The small-sized nanogels presumably reduced their contact with the surrounding H_2O molecules due to the amplified hydrophobicity of the system as the temperature increases, which allowed them to further aggregate with the pre-existing large ones. In the large nanoaggregates, a systematic downward transition of hydrodynamic radius (R_h) from 134 nm (at T = 25 °C) to 52 nm (at T = 55 °C) was detected. The particle size distributions (extracted from CONTIN analysis) are calculated as a function of the scattered intensity of different species in the solution, which is highly dependent on size. Accordingly, the number-weighted size distribution at T = 25 °C will be mostly represented by the small particles, while the distribution at T = 55 °C will be represented by the large ones (Figure 2b). This was also justified by the modest total mass at ambient temperature (as evidenced by the relatively low scattered intensity I = 106 kHz of the solution), which signifies the small portion of large aggregates and/or their loose, swollen structure. The hydrophobic interactions prevailed over the polymer–water ones during the thermal treatment, thereby producing relatively narrow size distributions (PDI = 0.262). On the other hand, Nanocarrier 2 demonstrated a rather less varied particle size from T = 25 °C (R_h = 75 nm) to T = 55 °C (R_h = 58 nm) (Figure 2d,e) with a modest change in scattered intensity, especially from T = 45 °C (I = 548 kHz) to T = 50 °C (I = 398 kHz), which is also associated with the amplified hydrophobicity of the particles and the expected tighter binding between the components.

The thermal treatment indicated that the lower critical solution temperature (LCST) point of the nanocarriers was shifted from 30 °C (for the copolymer [17]) to 45 °C, especially in the case of Nanocarrier 1. In Nanocarrier 2, hydrogen bonding and hydrophobic interactions drove the cross-linked network assembly, removing H_2O molecules from the network and thus shielding the hydrophilic-to-hydrophobic phase transition of the nanogel during temperature increase. A similar trend was presented in the work of Costa et al. [23]. The produced PNIPAAm-TA microgels with low TA concentration (5 wt% for neutral solutions) exhibited a shift of 3 °C to their LCST point compared to that of pure PNIPAAm microgels. In this regard, the hydrophilic character of TA also assisted the physicochemical alterations of polymer/TA complex behavior.

Yet the amphiphilic TA structures tend to be protonated/ionized at acidic/neutral conditions, respectively, due to the presence of catechol and pyrogallol moieties, further influencing the polymer/TA interactions. At alkaline conditions, the polyphenol groups are deprotonated, thus yielding unstable supramolecular TA/polymer assemblies [16,24]. According to DLS studies, it was revealed that both TA-based nanocarriers displayed pH-responsive characteristics, with Nanocarrier 2 exhibiting the most pronounced response to

pH change (Table 1). The neutral aqueous solution of Nanocarrier 1 comprised aggregates that scattered less (I = 106 kHz) compared to those of Nanocarrier 2 (I = 803 kHz). Furthermore, the intensity-weighted size distributions (bimodal for Nanocarrier 1 and monomodal for Nanocarrier 2) indicated the formation of loosely assembled copolymer–TA particles for Nanocarrier 1 (with R_h = 9 and 134 nm) and denser assembled particles for Nanocarrier 2 (R_h = 75 nm) (Figure 2b,e, T = 25 °C). As far as the responsiveness to acidic and basic conditions is concerned, Nanocarrier 1 revealed a slight collapse at pH = 3, judging by the decreased size observed in this pH value, while at pH =10, the aggregation phenomena led to the formation of particles with increased mass. On the other hand, Nanocarrier 2 demonstrated a remarkable response, especially in acidic conditions. The low pH caused disaggregation phenomena leading to the breaking of aggregates and liberation of copolymer chains (possibly those with dimethylamino groups that were further intramolecularly self-folded to unimers with an average hydrodynamic radius of ca. 3 nm). When the pH was adjusted to 10, partial collapse or destabilization of the nanocarrier was observed due to further deprotonation of DMAEMA units that provoked aggregation phenomena with the formation of small and large aggregates (R_h = 4 and 101 nm), most probably loose in structure (I = 301 kHz). Overall, the detected pH-responsive behavior of TA-based nanocarriers was noticeable at pH = 10, which is above the pKa of TA, ca. ~8.5, where hydrogen bonding is anticipated not to be active [25].

Table 1. Physicochemical characteristics of non-covalently cross-linked TA-based nanocarriers as assessed by DLS at θ = 90° and fluorescence spectroscopy at ambient temperature.

Sample	pH	I (kHz) [a]	R_h (nm) [b]	PDI [c]	I_1/I_3 [d]
Nanocarrier 1	3	103	8/75	0.62	1.68
	7	106	9/134	0.33	1.79
	10	518	11/83	0.49	1.53
Nanocarrier 2	3	104	3/96	0.54	1.74
	7	803	75	0.32	1.64
	10	301	4/101	0.39	1.39

[a] Determined by static light scattering (SLS) with 1–2% error. [b,c] Determined by dynamic light scattering (DLS) with a 5% error. [d] Determined by fluorescence spectroscopy.

Furthermore, the presence of ethylene glycol chains contributed to the stability of the formed nanocarriers in a neutral environment without precipitation or coacervation phenomena, even 20 days after preparation. Lee et al. [26] produced TA–hyaluronic acid hydrogels with enhanced stability as a result of the hydrogen bonding between TA and polyethylene glycol diglycidyl ether (PEGDE). The concentration of TA also affected the overall particle size distribution, especially in neutral conditions, where the compounding phase took place [23]. The higher the TA molar ratio, the higher the physical cross-linking density of the network was observed. In the case of Nanocarrier 1, rather polydisperse (PDI = 0.33) nanogel-type nanoaggregates with two different-sized particle populations (R_h = 9 and 134 nm) were observed, probably as a result of the insufficient quantity of cross-linker. Consequently, the cross-linker was not able to be efficiently distributed throughout the reaction volume during the mixing process. On the other hand, the TA concentration in Nanocarrier 2 was adequate for the available functional moieties of P(DMAEMA-co-OEGMA) to interact. The higher cross-linking suppressed the formation of smaller yet loosely bound species (compared to the ones observed in Nanocarrier 1) and resulted in a single population with more rigid structures. Al Nakeeb et al. [22] evaluated the effect of TA concentration on the self-assembly process of PVP-b-P(OEGMA) double-hydrophilic block copolymer. The collected bimodal intensity-weighted distributions (the results obtained from DLS) revealed aggregates of R_h = 15 nm and R_h = 300–400 nm, while the dissolution

in an alkaline environment led to disassembly phenomena as a result of hydrogen bonding breakdown between TA and PVP.

Finally, the polymer–TA nanocarriers were evaluated upon consecutive titrations with NaCl salt solution, producing solutions of different ionic strengths (Figure 2c,f). The NaCl concentration range (0.1–0.5 M) was selected to encompass physiological ionic strength (~0.15 M) and extend to supra-physiological conditions, enabling the assessment of electrostatic screening effects and nanocarrier robustness under ionic strength stress conditions. The aqueous solutions were titrated with NaCl 1 M at room temperature and pH = 7. Nanocarrier 1 demonstrated a remarkable downward trend in apparent molar mass, yet without significant particle size changes (Figure 2c), denoting a decrease in the mass and the density of the nanocarrier. It seems that the presence of NaCl salt at increasing concentration broke down the electrostatic and hydrogen bonding interactions between TA and mainly DMAEMA basic segments of the copolymer. On the contrary, Nanocarrier 2 (Figure 2f) showed only minor changes in the mass and size in the range of ionic strengths investigated. This could be a result of the higher ratio of TA relative to copolymer, which led to stronger bonding between the components, thus creating a more stable nanocarrier. Finally, the ionic strength studies demonstrated only a small amount of salt-induced responsiveness by both Nanocarriers, particularly at concentrations greater than those found in human blood (around 0.15 M). The negligible shifts in R_h and intensity (I) may be due to the hydrophobic polymeric network, which favors polymer–polymer interactions rather than between polymers and water molecules, which could result in swelling behavior.

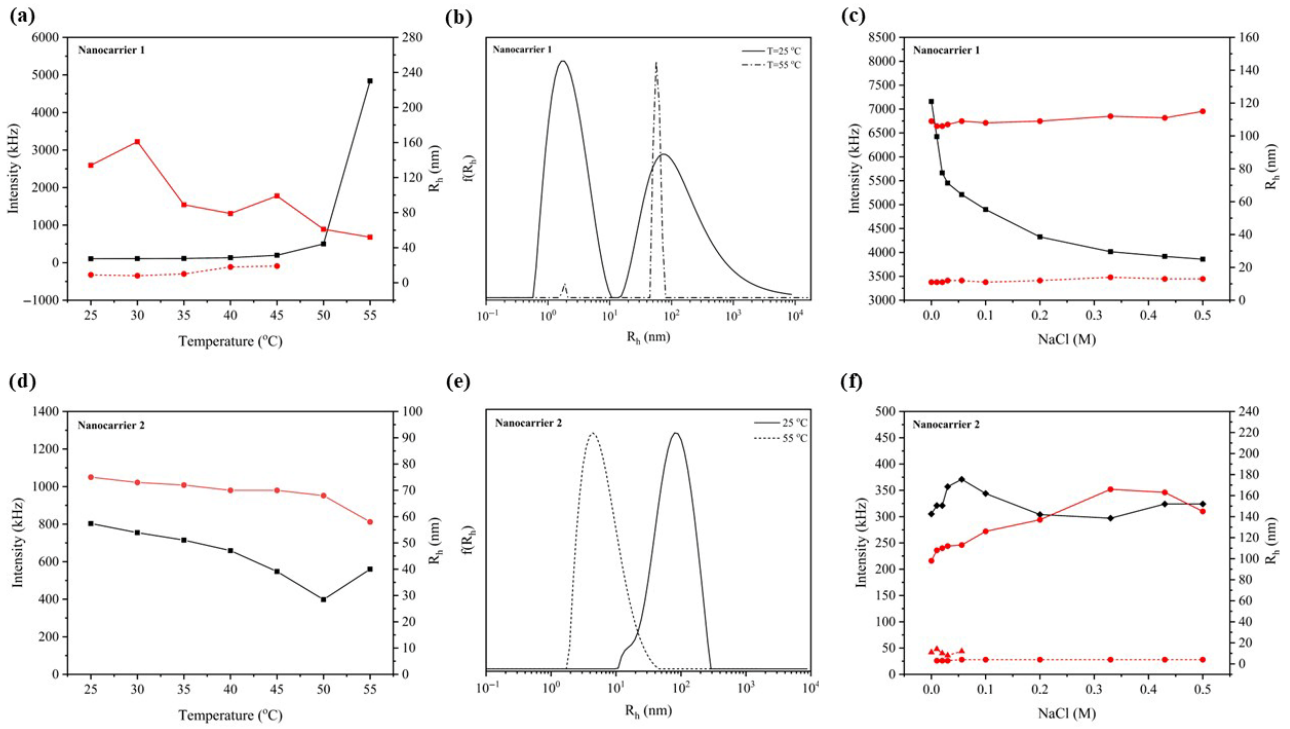


Figure 2. Correlation between the hydrodynamic radius (R_h) and scattered intensity (I) of Nanocarrier 1 and Nanocarrier 2 upon thermal treatment (**a**,**d**) and salt (NaCl 1 M) titrations (**c**,**f**), as well as (**b**,**e**) size distributions from CONTIN analysis at the two extreme temperatures (T = 25 °C and 55 °C) as determined by DLS (at pH = 7 and θ = 90°). The black lines correspond to scattered intensity, red lines to large-nanocarrier populations and red dotted lines to small nanocarriers.

3.2. Spectroscopic Characterization of TA-Based Nanocarriers

The TA-based nanocarriers were also studied by Fluorescence and UV-Vis spectroscopy to determine their spectral characteristics. Fluorescence spectroscopy was utilized in combination with the pyrene assay, as this is an effective method to evaluate the internal hydrophobicity and network conformation of the generated nanocarriers. Pyrene is a hydrophobic probe that gives information on the surrounding microenvironment and, consequently, the level of hydrophobicity/hydrophilicity within the physically cross-linked nanoaggregates formed. The micropolarity is estimated by the ratio (I_1/I_3) between the pyrene spectrum's first and third vibronic peaks [27]. Table 1 lists the I_1/I_3 ratios calculated at 25 °C for each nanocarrier in acidic, neutral, and alkaline conditions. In neutral aqueous solutions, Nanocarrier 1 revealed higher hydrophilicity (I_1/I_3 = 1.73) than Nanocarrier 2 (I_1/I_3 = 1.64). The intramolecular interactions with a higher amount of TA led to self-assembled nano-networks with higher cross-linking density that further shield the functional hydrophobic moieties from the hydrophilic surrounding media. Furthermore, the hydrophilic nature of internal micropolarity in acidic conditions was provoked by the protonation of the tertiary amine groups of the P(DMAEMA-co-OEGMA) copolymer. Likewise, in alkaline conditions, the relatively higher internal hydrophobicity was due to deprotonation of the amine groups. The observed quenching under those conditions (Figure S1), accompanied by decreased fluorescence intensity and an emission band at 500 nm, is potentially ascribed to the interactions between pyrene's excited state with the immediate surroundings within the nanocarriers [28].

UV-Vis spectroscopy measurements confirmed the effective hydrogen bonding between the biocompatible polymer and tannic acid (Figure 3). The P(DMAEMA-co-OEGMA) copolymer does not show measurable absorbance in the examined UV–Vis range, and therefore, the recorded spectra of the nanocarriers primarily reflect the presence and interactions of tannic acid with the random copolymer. The absorption peaks at 214 and 280 nm are associated with the aromatic groups of TA, whereas the peak at 256 nm could be attributed to the absorption by the phenol groups in the TA structure. TA absorption spectra in an aqueous acidic solution show two peaks at 214 and 271 nm, which are attributed to its neutral state. However, at higher pH values, these peaks are slightly shifted, accompanied by a shoulder at approximately 233 nm (which could belong to the phenolate form of TA) [24]. The UV-Vis spectra of the nanocarriers depicted in Figure 3 confirm the structural characteristics of the physically cross-linked nano-assemblies based on the aforementioned characteristics of the TA component.

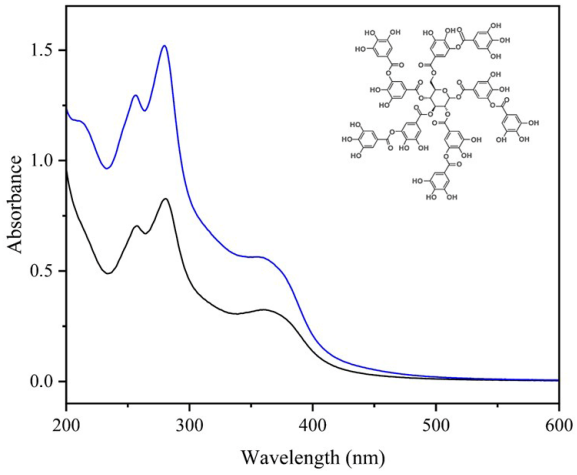


Figure 3. UV-Vis spectra of Nanocarrier 1 (black line) and Nanocarrier 2 (blue line). The presented chemical structure corresponds to the TA component.

3.3. Physicochemical Studies of TA-Based Nanocarriers Complexed with Ovalbumin

The hydrogen-bonded assembly of TA with various neutral polymers, including poly(N-vinylcaprolactam), poly(N-vinylpyrrolidone), poly(ethylene oxide), and PNIPAAm, has recently garnered increased attention for controlled drug/protein encapsulation/release applications [29]. Notably, the pH-sensitivity of TA-based networks facilitates the on-demand in vivo drug/protein delivery. Among others, Kim et al. [29] fabricated LBL films with PEO-b-PHEMA pH-responsive copolymer micelle of R_h = 192 nm for DOX (doxorubicin) accelerated release at pH = 4. The complexation process of such nanosystems with proteins relies on the intermolecular interactions between the TA moieties and biomacromolecules. In this regard, to avoid the strong hydrogen bonding between the phenolic hydroxyl groups of TA and carbonyl groups of proteins that could cause further functional modifications [30], the OVA molecules were complexed with the nanocarriers after P(DMAEMA-co-OEGMA)/TA intramolecular self-assembly.

The complexation studies were performed between TA–copolymer nanocarriers and ovalbumin (OVA) molecules at two mixes of protein weight contents (10% wt. and 20% wt.). The complexes were produced between the negative surface charge of ovalbumin molecules ($\zeta = -13 \pm 6$ mV) and the positive charge on each nanocarrier (Nanocarrier 1: $\zeta = +6.7 \pm 5.56$ mV and Nanocarrier 2: $\zeta = +20.1 \pm 2.95$ mV as determined by electrophoretic light scattering, ELS). The physicochemical characteristics of the TA-based copolymer nanocarriers complexed with OVA molecules (Table 2) revealed major differences between the nanocarriers. The complexes with Nanocarrier 1 displayed rather similar mass and bimodal particle size distribution with some heterogeneity. Given the fact that the Nanocarrier 1 formulation presented two different size distributions, the complexation with OVA molecules led to the creation of either small nanocomplexes (R_h = 3–4 nm) or free uncomplexed nanocarriers and of large-size complexes (R_h = 115–118 nm). Moreover, the smaller-scale species cannot be assigned to free OVA self-folding protein chains, since the native hydrodynamic radius of OVA molecules is lower in aqueous solutions (with/without salt). On the other hand, OVA complexation (10% wt.) with Nanocarrier 2 (Nanocarrier 2-10) revealed a rather homogenous aqueous solution with monomodal size distribution of presumably compact nanocomplexes with enhanced mass (I = 1274 kHz) compared to the parent nanocarrier. On the contrary, Nanocarrier 2-20 complexation with OVA resulted in a trimodal size distribution with potentially small complexes or uncomplexed nanocarriers (R_h = 2 and 5 nm) and large-sized ones (R_h = 117 nm). Moreover, the negligible differentiation among the surface charges of OVA/nanocarrier complexes highlighted the formation of potentially stable aqueous solutions.

Table 2. Physicochemical characteristics of electrostatically formed complexes of OVA with TA–copolymer nanocarriers as assessed by DLS, at $\theta = 90^\circ$, and ELS.

Sample	I (kHz) [a]	R_h (nm) [b]	PDI [c]	ζ-Potential (mV) [d]
Nanocarrier 1-10	34	3/118	0.533	35.1 ± 4.94
Nanocarrier 1-20	31	4/115	0.609	30.3 ± 2.79
Nanocarrier 2-10	1274	96	0.141	36.8 ± 3.38
Nanocarrier 2-20	73	2/5/117	0.407	32.1 ± 3.03

[a] Determined by static light scattering (SLS) with 1–2% error. [b,c] Determined by dynamic light scattering (DLS) with a 5% error. [d] Determined by electrophoretic light scattering (ELS).

The thermal treatment of TA-based nanocarriers complexed with OVA showed the absence of thermal responsiveness, further corroborating the strong complexation of the components driven by electrostatic interactions (Figure S2). Eventually, the temperature-

stable nanocarriers could protect the protein molecules from denaturation and maintain their biological functionalities upon delivery.

Studies on the function of solution ionic strength were subsequently conducted to examine the response of complexes after consecutive salt additions, comparable to those in human blood (~0.15 M) and above. For Nanocarrier 1/OVA complexes, a moderate increase in scattered intensity and hydrodynamic radius was detected, originating from the salting-out effects that provoke aggregation phenomena. Specifically, a slight increase in both parameters was detected after the first salt addition (C_{NaCl} ~ 0.1 M) in the case of Nanocarrier 1-10 (Figure 4a), while an upward trend was observed for Nanocarrier 1-20 (Figure 4b). The most intense growth was located from 0.2 M to 0.5 M, yet at a higher concentration than that of human blood. Conversely, the Nanocarrier 2-10 complexes (Figure 4c) showed a significant decrease in scattered intensity following the second salt addition (roughly at 0.1 M NaCl) but displayed rather constant mass to further increases in solution ionic strength. Size (R_h) was also decreased, suggesting partial complex collapse, followed by the emergence of small-size complexes from 0.1 M to 0.43 M with R_h = 8–11 nm. The formation of these small-nanocarrier/OVA complexes could be ascribed either to the weakening of the interactions between the components or to the screening of the electrostatic interactions that cause partial destabilization/collapse and reorganization of the physically cross-linked network. Finally, Nanocarrier 2-20 showed an overall upward tendency. The apparent mass was reduced after the first salt addition (decrease in intensity), potentially due to the weakening of electrostatic interactions, but followed a moderate growth from C_{NaCl} ~ 0.2 M (I = 42 kHz) and onwards (I = 62 kHz, C_{NaCl} ~ 0.5 M) (Figure 4d).

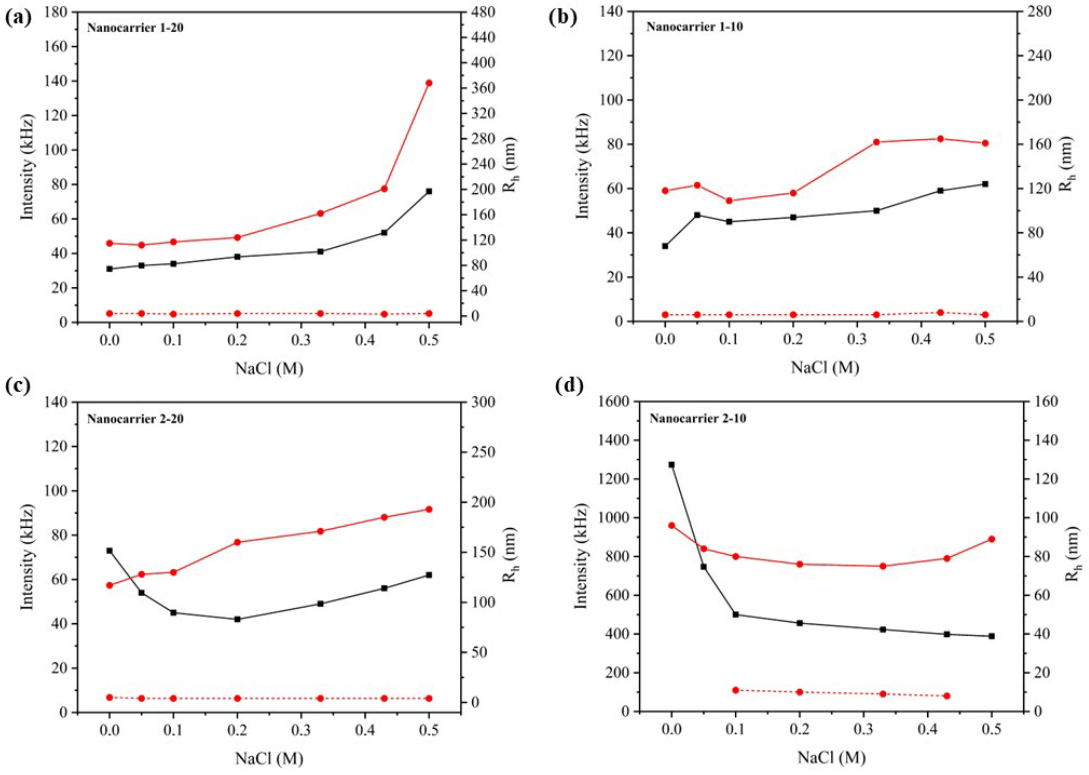


Figure 4. Salt-induced responsiveness of nanocarrier/OVA complexes as detected by DLS measurements. (**a**–**d**) intensity and R_h graphs vs NaCl concentration for different nanocarriers. The black lines correspond to the scattered intensity, red lines to large-size nanocarrier/OVA complexes and red dotted lines to small-size ones.

Stability studies of the nanocarrier/OVA complexes over storage and upon dilution with different serum concentrations (FBS/PBS) were also conducted to assess the robustness

of these systems. Nanocarrier 1/OVA complexes were detected with rather amplified kinetic stability during a storage period of 20 days at ambient conditions (Figure 5). On the other hand, Nanocarrier 2/OVA complexes exhibited a systematic collapse accompanied by disaggregation phenomena, thus rendering these complex systems unstable over time. Notably, Nanocarrier 2-10 disintegrated into two populations after the 10th day.

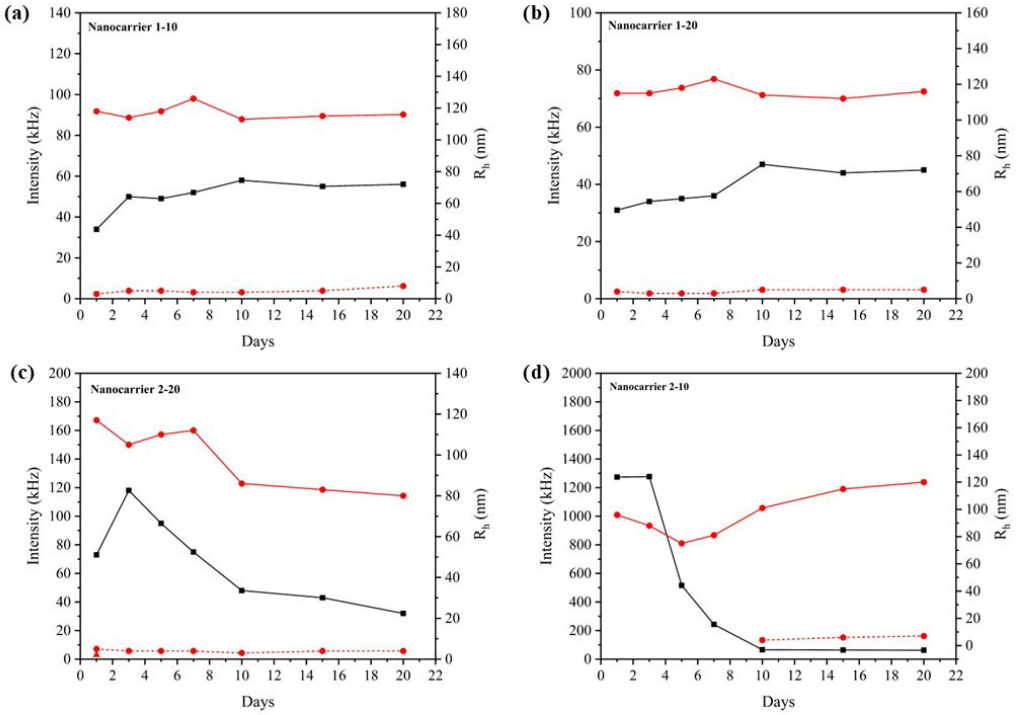


Figure 5. Scattered intensity (black lines) and hydrodynamic radius (red line for large complexes and red dotted line for small ones) as a function of time for nanocarrier/OVA complexes (**a**) Nanocarrier 1-10, (**b**) Nanocarrier 1-20, (**c**) Nanocarrier 2-10 and (**d**) Nanocarrier 2-20 as detected by DLS measurements.

Different FBS:PBS ratios were employed to simulate protein-rich and protein-diluted biological environments to evaluate the stability of the nanocarrier/OVA complexes under varying serum concentrations. The trimodal size distribution revealed by the DLS data illustrates the heterogeneity of the FBS medium utilized as a blood simulation environment for assessing the biological stability and compatibility of the nanocarrier/OVA complexes. The peaks for 1:10 FBS/PBS mixtures were about 4 nm, 12 nm, and 73 nm, whereas the peaks for 1:2 FBS/PBS mixtures were around 3 nm, 13 nm, and 70 nm. The smaller species potentially correspond to single proteins, while the larger species were thought to belong to protein clusters/aggregates. These results indicated that the dilution with PBS buffer had no discernible effects. According to the size distributions obtained at T = 25 °C (Figure 6), (Tables S1 and S2), there were no appreciable increases in the sizes of the existing nanocarrier populations when comparing the initial size distributions of the nanocarrier/OVA complexes with the ones obtained after mixing with FBS/PBS solutions. Consequently, it can be claimed that in both FBS solutions (1:1 v/v and 1:10 v/v with PBS), there were no significant interactions between the complexes and serum proteins. Furthermore, the interactions at simulated human temperature (T = 37 °C) did not exhibit remarkable differences regarding the particle size distribution upon interaction with serum proteins. This behavior should be attributed to the presence of oligoethylene oxide-type OEGMA segments, side chains that shield the nanostructures in aqueous media.

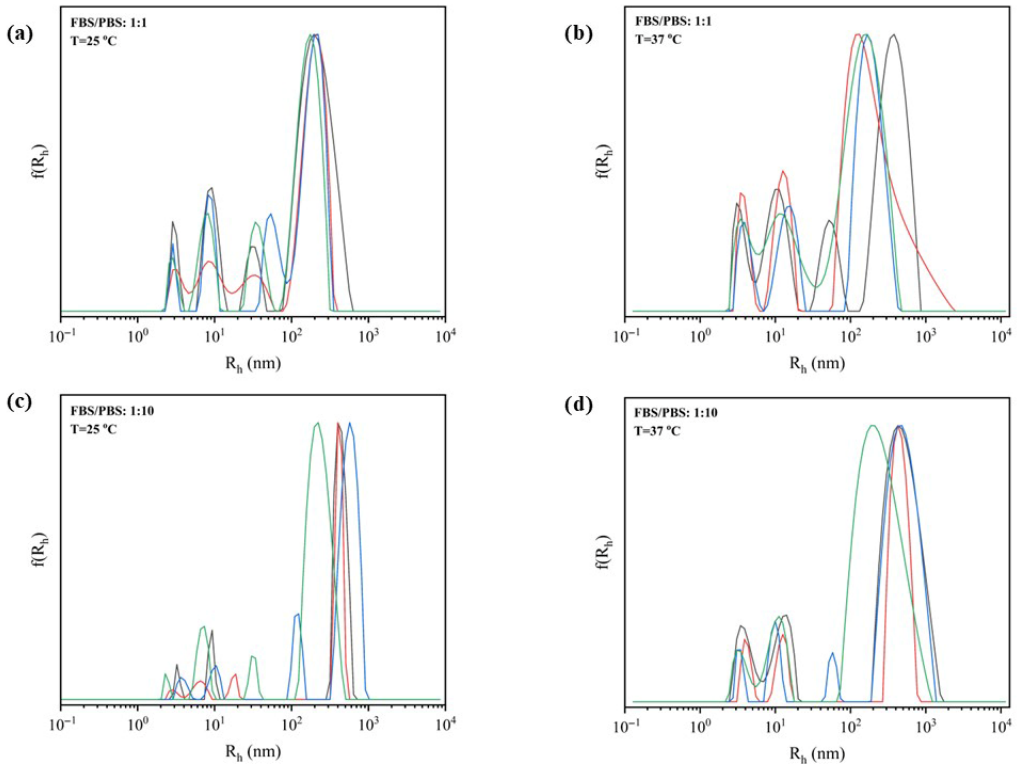


Figure 6. Intensity-weighted size distributions of Nanocarrier 1-10 (black line), Nanocarrier 1-20 (red line), Nanocarrier 2-10 (blue line) and Nanocarrier 2-20 (green line) upon dilution with FBS: PBS 1:1 v/v (**a**,**b**) and 1:10 v/v (**c**,**d**) as determined by DLS measurements at T = 25 °C and T = 37 °C.

Overall, Nanocarrier 1/OVA complexes displayed heterogeneous mass and bimodal particle size distribution, leading to the formation of small nanocomplexes or large-scale ones. In contrast, Nanocarrier 2 exhibited monomodal or trimodal size distributions, indicating different complexation structures, especially at zero time (i.e., immediately after mixing). Salinity alterations revealed moderate changes in scattered intensity and hydrodynamic radius, with Nanocarrier 1 complexes showing aggregation at higher salt concentrations, while Nanocarrier 2 complexes exhibited partial collapse and reorganization of the physically cross-linked network due to electrostatic screening, rather than complete disassembly. These findings suggest the importance of electrostatic interactions in driving complexation and highlight the potential of temperature-stable nanocarriers for protein delivery applications.

Colloidal stability was verified only in the case of Nanocarrier 1/OVA complexes, where they did not significantly alter as far as their particle size and mass are concerned. The complex systems potentially reached a dynamic equilibrium despite the solution heterogeneity, contributing to their potential application as nanocarriers for negatively charged proteins. The detected stability could be ascribed to the presence of OEGMA segments, which shield the nanocarriers with lengthy side chains of hydrophilic ethylene oxide units. Furthermore, the obtained surface charges of the OVA/nanocarrier complexes were within the desired range of zeta potentials for maintaining the stability of colloidal systems stabilized through a combination of steric and electrostatic interactions [31]. However, the high positive surface charge of the nanocarrier/OVA complexes prepared in the current study could be a disadvantage in terms of immune recognition, macrophage uptake and protein binding [32]. In order to improve biocompatibility while maintaining colloidal stability, future designs could modulate the surface charge by adjusting the copolymer composition or architecture, such as by increasing OEGMA content, adding alternative OEGMA segments with varying lengths of ethylene oxide side chains, adding PEG-based

shielding layers, or utilizing zwitterions for partial interaction with DMAEMA segments before physical cross-linking. Aquilera et al. [33] designed TA nanoparticles (NPs) coated with PEG and a recombinant protein A (rPA) with a PEG-binding domain that facilitates the binding of the antibody in the appropriate orientation. The TA/PEG NPs displayed an average R_h = 330 nm and $\zeta = -21$ mV, which is identical to the surface charge of the naked TA, indicating the formation of colloidal stable antibody-based nanocarriers with a size relevant to the molecular weight of the polymer. In spite of having a high positive surface charge, Nanocarrier 2/OVA complexes proved unstable, judging from the disintegration phenomena. The reduced stability of the Nanocarrier 2/OVA complexes may be attributed to the high tannic acid content, which promoted heterogeneous yet dense assemblies with limited structural adaptability of the polymeric network. This structural rigidity (dense hydrogen bonding clusters, TA-TA domains and complexed OVA molecules) also led to slow structural relaxation and structural reorganization during prolonged storage. Thus, these behaviors suggested that an optimal balance between TA content, electrostatic interactions and hydrophobic stabilization is required to achieve long-term stability. To conclude, it should be noted that the physicochemical studies upon complexation with serum proteins (FBS/PBS) verified negligible interactions with serum proteins and minimal structural changes. The absence of significant size increase or aggregation phenomena, either at physiological conditions (25 °C) or at human simulated temperature (37 °C), in the presence of serum proteins, suggested limited protein absorption, which may help to preserve the colloidal integrity upon exposure to biological fluids. This behavior is commonly associated with reduced optonization and better biodistribution profiles in vivo.

3.4. Structural Studies of Electrostatically Complexed OVA

UV absorbance of proteins (300–400 nm) is attributed to the contained tryptophan, tyrosine, and phenylalanine, more hydrophobic amino acids (with tryptophan being the most active). Therefore, the absence of a shift to wavelengths greater than 280 nm subsequently suggests that substantial conformational changes did not take place throughout the complexation process. The tryptophan UV absorption of nanocarrier/OVA complexes did not significantly vary, with the peak of tryptophan residue at λ_{max} = 280 nm being particularly difficult to interpret. The aromatic groups of TA also strongly absorb in the same UV region, as analyzed in Section 3.2, obstructing the signal of OVA molecules and thereby masking the potential absorbance differences arising from different protein concentrations. It is noteworthy that the absorption peak of aromatic acids at 214 nm in the nanocarrier spectrum has disappeared in the spectrum of complexes, thus corroborating the successful complexation with protein molecules (Figure 7a). Studies using fluorescence spectroscopy, which qualitatively analyzes the tertiary structure of protein molecules, revealed a weak signal from the integrated protein. The tryptophan amino acid fluorescence signals were not strong enough to confirm that no conformational changes were provoked after the complexation process. Hence, it is not very safe to draw firm conclusions about the protein structure.

Furthermore, using ATR-FTIR spectra, it was possible to qualitatively determine if complexed OVA molecules are completely or partially disordered. Following complexation with the TA-based nanocarriers, the representative amide I (1635 cm^{-1}) and amide II (1586 cm^{-1}) peaks showed a consistent frequency, indicating that the secondary structure of OVA molecules remained unchanged (Figure 7b). The differences between the ATR intensities were ascribed to the relative concentration of vibrationally active functional groups rather than to conformational changes of the protein. Moreover, the absence of significant shifts or broadening of the amide I and II bands further supported that OVA molecules did not undergo denaturation upon electrostatic complexation with the

copolymer nanocarriers. The polymeric network of the nanogel was correlated with the significant vibration of the carbonyl and ether groups detected in the spectra.

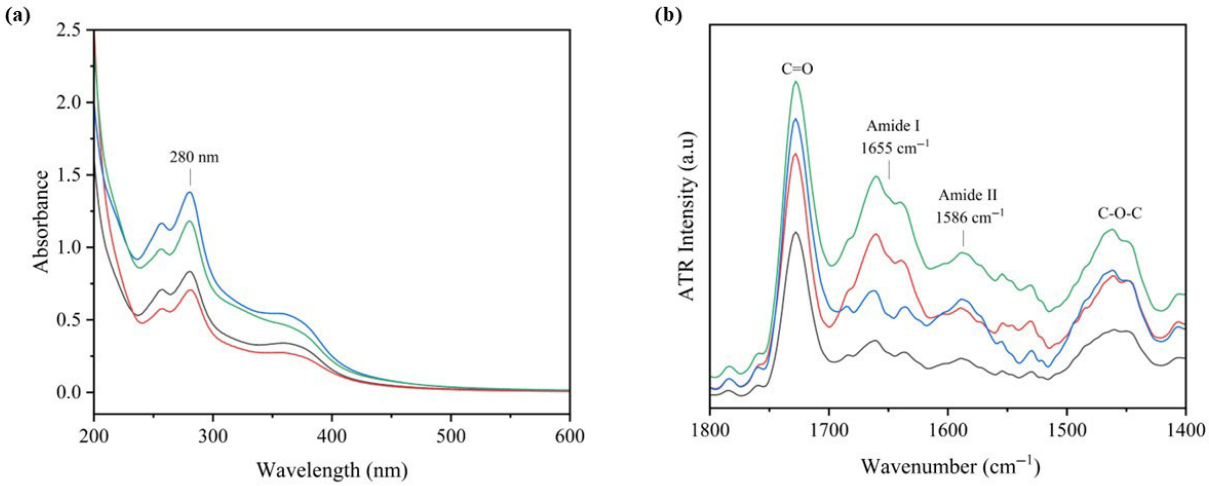


Figure 7. (**a**) UV-Vis and (**b**) FTIR-ATR spectrum of Nanocarrier 1-10 (black line), Nanocarrier 1-20 (red line), Nanocarrier 2-10 (blue line) and Nanocarrier 2-20 (green line).

4. Conclusions

In conclusion, our study highlights the successful formation of TA-based nanocarriers through the self-assembly by physical cross-linking of P(DMAEMA-co-OEGMA) random copolymer and tannic acid (TA), facilitated by electrostatic interactions, hydrogen bonding and hydrophobic interactions. The resulting complexes exhibited diverse physicochemical properties depending on TA concentration, with Nanocarrier 1 displaying heterogeneity and bimodal particle size distribution with R_h = 9 and 134 nm, while Nanocarrier 2 exhibited monomodal size distribution (R_h = 75) nm under neutral solution conditions. Studies on the effect of salinity revealed differing responses to salt concentration, with Nanocarrier 2 complexes showing aggregation at higher salt concentrations than that of human blood (0.15 M), whereas Nanocarrier 1 complexes exhibited partial collapse followed by disintegration phenomena. Furthermore, the evaluation of TA-based nanocarriers and ovalbumin complexes revealed different states of complexation. The physicochemical characterization further confirmed the eligibility of these complexes for potential biomedical applications, highlighting their stability in the presence of serum proteins and their size and surface charge within desired ranges. Nonetheless, despite the instability over time and in salt concentrations higher than 0.15 M observed in Nanocarrier 2/OVA complexes, Nanocarrier 1/OVA complexes maintained colloidal stability, rendering them promising nanocarriers for negatively charged proteins.

Overall, through comprehensive physicochemical analysis, we delineated the diverse characteristics of the resulting TA–copolymer nanocarriers and nanocarrier/OVA complexes. These observations underscore the critical necessity of assessing the complexity of nanocarrier formation through TA-induced cross-linking to optimize protein complexation and structure. Such insights are pivotal in crafting advanced drug delivery systems capable of shielding protein integrity and functionality during encapsulation and delivery.

Supplementary Materials: The following supporting information can be downloaded at: https://www.mdpi.com/article/10.3390/macromol6010017/s1, Figure S1: Fluorescence spectra of pyrene in the presence of (a) Nanocarrier 1 and (b) Nanocarrier 2 at different pH values (red line: pH = 3, black line: pH = 7, blue line: pH = 10)., Figure S2: Temperature responsiveness of (a) Nanocarrier 1-10, (b) Nanocarrier 1-20, (c) Nanocarrier 2-10 and (d) Nanocarrier 2-20. The black lines correspond to scattered light intensity measurements, the red lines to large complexes and dashed red lines and

single dot in (c) to small-size complexes; Table S1: Physicochemical properties of Nanocarriers/OVA complexes in 1:1 FBS/PBS, as determined by DLS experiments; Table S2: Physicochemical properties of Nanocarriers/OVA complexes with 1:10 FBS/PBS, as determined by DLS experiments.

Author Contributions: Conceptualization, S.P.; investigation, A.V.; data curation, A.V.; writing—review and editing, A.V. and S.P.; supervision, S.P.; project administration, S.P. All authors have read and agreed to the published version of the manuscript.

Funding: This research received no external funding.

Institutional Review Board Statement: Not applicable.

Informed Consent Statement: Not applicable.

Data Availability Statement: The raw data supporting the conclusions of this article will be made available by the authors on request.

Conflicts of Interest: The authors declare no conflicts of interest.

References

1. Varanko, A.; Saha, S.; Chilkoti, A. Recent trends in protein and peptide-based biomaterials for advanced drug delivery. *Adv. Drug Deliv. Rev.* **2020**, *156*, 133–187. [CrossRef]
2. Deb, P.K.; Al-Attraqchi, O.; Chandrasekaran, B.; Paradkar, A.; Tekade, R.K. Protein/peptide drug delivery systems: Practical considerations in pharmaceutical product development. In *Basic Fundamentals of Drug Delivery*; Elsevier: Amsterdam, The Netherlands, 2019; pp. 651–684.
3. Awwad, S.; Ginn, C.; Brocchini, S. 2—The case for protein PEGylation. In *Engineering of Biomaterials for Drug Delivery Systems*; Parambath, A., Ed.; Woodhead Publishing: Thornton, UK, 2018; pp. 27–49.
4. Li, C.; Li, T.; Tian, X.; An, W.; Wang, Z.; Han, B.; Tao, H.; Wang, J.; Wang, X. Research progress on the PEGylation of therapeutic proteins and peptides (TPPs). *Front. Pharmacol.* **2024**, *15*, 1353626. [CrossRef] [PubMed]
5. Hoang Thi, T.T.; Pilkington, E.H.; Nguyen, D.H.; Lee, J.S.; Park, K.D.; Truong, N.P. The Importance of Poly(ethylene glycol) Alternatives for Overcoming PEG Immunogenicity in Drug Delivery and Bioconjugation. *Polymers* **2020**, *12*, 298. [CrossRef] [PubMed]
6. Le Saux, S.; Aubert-Pouëssel, A.; Ouchait, L.; Mohamed, K.E.; Martineau, P.; Guglielmi, L.; Devoisselle, J.-M.; Legrand, P.; Chopineau, J.; Morille, M. Nanotechnologies for Intracellular Protein Delivery: Recent Progress in Inorganic and Organic Nanocarriers. *Adv. Ther.* **2021**, *4*, 2100009. [CrossRef]
7. Jash, A.; Ubeyitogullari, A.; Rizvi, S.S.H. Liposomes for oral delivery of protein and peptide-based therapeutics: Challenges, formulation strategies, and advances. *J. Mater. Chem. B* **2021**, *9*, 4773–4792. [CrossRef]
8. Vardaxi, A.; Kafetzi, M.; Pispas, S. Polymeric nanostructures containing proteins and peptides for pharmaceutical applications. *Polymers* **2022**, *14*, 777. [CrossRef]
9. Honda, Y.; Nomoto, T.; Matsui, M.; Takemoto, H.; Kaihara, Y.; Miura, Y.; Nishiyama, N. Sequential self-assembly using tannic acid and phenylboronic acid-modified copolymers for potential protein delivery. *Biomacromolecules* **2020**, *21*, 3826–3835.
10. Kaczmarek, B. Tannic acid with antiviral and antibacterial activity as a promising component of biomaterials—A minireview. *Materials* **2020**, *13*, 3224. [CrossRef]
11. Chowdhury, P.; Nagesh, P.K.B.; Hatami, E.; Wagh, S.; Dan, N.; Tripathi, M.K.; Khan, S.; Hafeez, B.B.; Meibohm, B.; Chauhan, S.C.; et al. Tannic acid-inspired paclitaxel nanoparticles for enhanced anticancer effects in breast cancer cells. *J. Colloid Interface Sci.* **2019**, *535*, 133–148. [CrossRef]
12. Shin, M.; Lee, H.-A.; Lee, M.; Shin, Y.; Song, J.-J.; Kang, S.-W.; Nam, D.-H.; Jeon, E.J.; Cho, M.; Do, M.; et al. Targeting protein and peptide therapeutics to the heart via tannic acid modification. *Nat. Biomed. Eng.* **2018**, *2*, 304–317. [CrossRef]
13. Popa, M.; Constantin, C.; Ochiuz, L.; Desbrieres, J.; Peptu, C. Controlling the release kinetics of calcein loaded liposomes from chitosan/tannic acid and chitosan/poly (vinyl alcohol)/tannic acid hydrogels. *Cellulo Chem. Technol* **2018**, *52*, 353–370.
14. Kumorek, M.; Minisy, I.M.; Krunclová, T.; Voršiláková, M.; Venclíková, K.; Chánová, E.M.; Janoušková, O.; Kubies, D. pH-responsive and antibacterial properties of self-assembled multilayer films based on chitosan and tannic acid. *Mater. Sci. Eng. C* **2020**, *109*, 110493. [CrossRef] [PubMed]
15. Mohammadi, M.; Salami-Kalajahi, M.; Roghani-Mamaqani, H.; Golshan, M. Effect of molecular weight and polymer concentration on the triple temperature/pH/ionic strength-sensitive behavior of poly(2-(dimethylamino)ethyl methacrylate). *Int. J. Polym. Mater. Polym. Biomater.* **2017**, *66*, 455–461. [CrossRef]
16. Chen, C.; Yang, H.; Yang, X.; Ma, Q. Tannic acid: A crosslinker leading to versatile functional polymeric networks: A review. *RSC Adv.* **2022**, *12*, 7689–7711. [CrossRef]

17. Vardaxi, A.; Pispas, S. Stimuli-Responsive Self-Assembly of Poly(2-(Dimethylamino)ethyl Methacrylate-co-(oligo ethylene glycol)methacrylate) Random Copolymers and Their Modified Derivatives. *Polymers* **2023**, *15*, 1519. [CrossRef]
18. Tian, Y.; Bian, S.; Yang, W. A redox-labile poly (oligo (ethylene glycol) methacrylate)-based nanogel with tunable thermosensitivity for drug delivery. *Polym. Chem.* **2016**, *7*, 1913–1921. [CrossRef]
19. Kafetzi, M.; Pispas, S.; Bao, X.; Yao, P. Amphiphilic QP(DMAEMA-co-LMA)-b-POEGMA Random-Block Terpolymers as Nanocarriers for Insulin. *Biomedicines* **2020**, *8*, 392. [CrossRef]
20. Zhang, L.; Nguyen, T.L.U.; Bernard, J.; Davis, T.P.; Barner-Kowollik, C.; Stenzel, M.H. Shell-Cross-Linked Micelles Containing Cationic Polymers Synthesized via the RAFT Process: Toward a More Biocompatible Gene Delivery System. *Biomacromolecules* **2007**, *8*, 2890–2901. [CrossRef]
21. Chrysostomou, V.; Katifelis, H.; Gazouli, M.; Dimas, K.; Demetzos, C.; Pispas, S. Hydrophilic Random Cationic Copolymers as Polyplex-Formation Vectors for DNA. *Materials* **2022**, *15*, 2650. [CrossRef]
22. Al Nakeeb, N.; Nischang, I.; Schmidt, B.V. Tannic Acid-Mediated Aggregate Stabilization of Poly (N-vinylpyrrolidone)-b-poly (oligo (ethylene glycol) methyl ether methacrylate) Double Hydrophilic Block Copolymers. *Nanomaterials* **2019**, *9*, 662. [CrossRef]
23. Costa, E.; Coelho, M.; Ilharco, L.M.; Aguiar-Ricardo, A.; Hammond, P.T. Tannic Acid Mediated Suppression of PNIPAAm Microgels Thermoresponsive Behavior. *Macromolecules* **2011**, *44*, 612–621. [CrossRef]
24. Shutava, T.; Prouty, M.; Kommireddy, D.; Lvov, Y. pH Responsive Decomposable Layer-by-Layer Nanofilms and Capsules on the Basis of Tannic Acid. *Macromolecules* **2005**, *38*, 2850–2858. [CrossRef]
25. Erel-Unal, I.; Sukhishvili, S.A. Hydrogen-Bonded Multilayers of a Neutral Polymer and a Polyphenol. *Macromolecules* **2008**, *41*, 3962–3970. [CrossRef]
26. Lee, H.-Y.; Hwang, C.-H.; Kim, H.-E.; Jeong, S.-H. Enhancement of bio-stability and mechanical properties of hyaluronic acid hydrogels by tannic acid treatment. *Carbohydr. Polym.* **2018**, *186*, 290–298. [CrossRef] [PubMed]
27. Vardaxi, A.; Forys, A.; Trzebicka, B.; Pispas, S. Nanogel-type nano-objects from a random polyelectrolyte through intermolecular cross-linking. *Nano-Struct. Nano-Objects* **2024**, *38*, 101122. [CrossRef]
28. Piñeiro, L.; Novo, M.; Al-Soufi, W. Fluorescence emission of pyrene in surfactant solutions. *Adv. Colloid Interface Sci.* **2015**, *215*, 1–12. [CrossRef]
29. Kim, B.-S.; Lee, H.-i.; Min, Y.; Poon, Z.; Hammond, P.T. Hydrogen-bonded multilayer of pH-responsive polymeric micelles with tannic acid for surface drug delivery. *Chem. Commun.* **2009**, 4194–4196. [CrossRef]
30. Yang, S.; Wang, Y.; Wu, X.; Sheng, S.; Wang, T.; Zan, X. Multifunctional tannic acid (TA) and lysozyme (lys) films built layer by layer for potential application on implant coating. *ACS Biomater. Sci. Eng.* **2019**, *5*, 3582–3594. [CrossRef]
31. Pippa, N.; Pippa, N.; Pispas, S.; Demetzos, C. Physico-chemical Characterization and Basic Research Principles of Advanced Drug Delivery Nanosystems. In *Intelligent Nanomaterials*; Wiley: Hoboken, NJ, USA, 2016; pp. 107–125.
32. Duan, X.; Li, Y. Physicochemical Characteristics of Nanoparticles Affect Circulation, Biodistribution, Cellular Internalization, and Trafficking. *Small* **2013**, *9*, 1521–1532. [CrossRef]
33. Aguilera, J.; Venegas, V.; Oliva, J.M.; Sayagués, M.J.; De Miguel, M.; Sánchez-Alcázar, J.A.; Arévalo-Rodríguez, M.; Zaderenko, A. Targeted multifunctional tannic acid nanoparticles. *RSC Adv.* **2016**, *6*, 7279–7287. [CrossRef]

Disclaimer/Publisher's Note: The statements, opinions and data contained in all publications are solely those of the individual author(s) and contributor(s) and not of MDPI and/or the editor(s). MDPI and/or the editor(s) disclaim responsibility for any injury to people or property resulting from any ideas, methods, instructions or products referred to in the content.